

000 001 002 003 004 005 COLD-STEER: STEERING LARGE LANGUAGE MODELS 006 VIA IN-CONTEXT ONE-STEP LEARNING DYNAMICS 007 008 009

010 **Anonymous authors**
011 Paper under double-blind review
012
013
014
015
016
017
018
019
020
021
022
023
024
025
026
027
028
029
030

ABSTRACT

031 Activation steering methods enable inference-time control of large language model
032 (LLM) behavior without retraining, but current approaches either capture subop-
033 timally steering signals from labeled examples or require hundreds to thousands
034 of examples to optimize using specific procedures for each behavioral target. We
035 introduce COLD-Steer, a training-free framework that steers LLM activations by
036 approximating the representational changes that would result from gradient descent
037 on in-context examples. Our key insight is that the effect of fine-tuning on a small
038 set of examples can be efficiently approximated at inference time without actual
039 parameter updates. We formalize this through two complementary approaches: (i)
040 a unit kernel approximation method that updates the activations directly using
041 gradients with respect to them, normalized across examples, and (ii) a finite-difference
042 approximation requiring only two forward passes regardless of example count.
043 Experiments across a variety of steering tasks and benchmarks demonstrate that
044 COLD-Steer achieves upto 95% steering effectiveness while using 50 times fewer
045 samples compared to the best baseline. COLD-Steer enables real-time adaptation
046 to new steering objectives and facilitates accommodating diverse perspectives with-
047 out extensive demonstration data, which we validate through our experiments on
048 pluralistic alignment tasks. Our framework opens new possibilities for adaptive,
049 context-aware model control that can flexibly address varying loss-driven human
050 preferences through principled approximation of learning dynamics rather than
051 specialized training procedures.
052
053

1 INTRODUCTION

034
035
036
037 What if we could steer a language model’s behavior with as few examples as we’d use to teach a
038 human – tens of demonstrations instead of hundreds? Consider steering a model from generating:
039 *As a woman, she was naturally emotional in the workplace* → *As a professional, she maintained*
040 *composure in the workplace*. Current activation steering methods would require anywhere between
041 250 to 1000 examples to **effectively** learn this intervention, yet humans grasp such behavioral shifts
042 from just a handful of cases. This gap reveals a fundamental inefficiency in current model control.

043 LLMs encode concepts as directions in high-dimensional activation spaces that causally shape their
044 behavior. This perspective reframes the alignment problem: rather than retraining entire models or
045 crafting complex prompts, we can perform targeted interventions on these causal pathways during
046 inference (Elhage et al., 2021; Wang et al., 2022; Mitchell et al., 2022). However, existing activation
047 steering methods (Olah et al., 2020; Park et al., 2023; Marks & Tegmark, 2023; Gurnee & Tegmark,
048 2023; Cunningham et al., 2023; Ghandeharioun et al., 2024; Pan et al., 2024; Wu et al., 2024) face a
049 critical tradeoff between being sample efficient and learning a generalized steering signal. Parameter-
050 tuning approaches like ReFT (Wu et al., 2024) train some parameters to learn effective transformations
051 over these representations but require hundreds of examples to accurately identify these directions.
052 On the other hand, contrastive approaches like CAA (Panickssery et al., 2023) are more robust
053 to the number of samples but rely on activation-only signals of positive-negative pairs, which is
often ineffective in practice. Figure 1 reveals this fundamental trade-off: high steerability demands
extensive data and training, while efficient methods sacrifice control precision. This dichotomy stems

054

055

056

057

058

059

060

061

062

063

064

065

066

067

068

069

070

071

072

Steering method	Optimization-free	Sample-efficient	Behavioral target	Steering Signal
Prompt tuning (Brown et al., 2020a)	✗	✓	Prompt-driven	Implicit
Contrastive (Panickser et al., 2023; Liu et al., 2023; Zou et al., 2023)	✓	✓	Positive-negative pairs	Activation
Parameter tuning (Cao et al., 2024; Wu et al., 2024)	✗	✗	Loss-driven	Gradient
COLD (proposed)	✓	✓	Loss-driven	Gradient

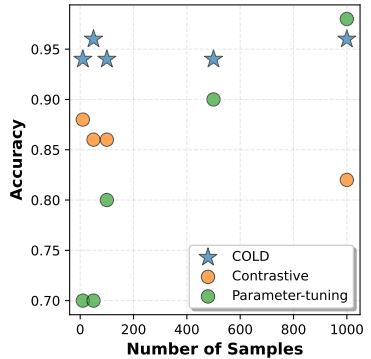


Figure 1: Comparison of steering methods based on their efficiency and steerability. The adjoining figure shows a representative trend for steering accuracy versus number of samples.

from treating steering as a static optimization problem, *i.e.*, find the one direction that works for all inputs rather than leveraging the model’s own learning mechanisms¹.

Our key insight lies in the fact that when models learn from examples during fine-tuning, they create predictable changes in their representation. Recent work on learning dynamics (Ren & Sutherland, 2024; Arora et al., 2019) shows these changes follow analyzable patterns. This highlights a transformative alternative – instead of collecting hundreds of examples to enable steering, one can compute how the model would learn from just a few in-context examples Brown et al. (2020b) and apply that transformation directly to activations. This entails no training, just simulating the effect of learning. To this end, we introduce **COLD-Steer**: steering via in-Context One-step Learning Dynamics, a novel optimization-free, activation steering framework that explicitly models how gradient updates from contextual examples would affect intermediate representations, enabling targeted causal intervention during inference. We provide two complementary methods: (1) COLD-Kernel-Steer, which aggregates learning effects through kernel-weighted combinations, and (2) COLD-FD-Steer, which approximates gradients via finite differences.

Our approach naturally unifies existing contrastive methods, as we show that CAA implicitly estimates the direction that gradient descent for a particular loss function, when computing the difference between positive and negative activations. Furthermore, our sample efficiency makes pluralistic alignment (Sorensen et al., 2024b; Santurkar et al., 2023), *i.e.*, adapting to varied human values, practically achievable. We rigorously evaluate our approach against existing steering methods to generate the desired behavior across various LLMs and datasets. Figure 1 demonstrates the practical impact: our method achieves comparable or superior steering accuracy with 10-50× fewer examples. By re-conceptualizing steering as simulated learning, COLD-Steer bridges the gap between the theoretical understanding of how models encode behaviors and the practical need for efficient, adaptable control mechanisms, thereby opening new avenues for model control.

2 PROBLEM

Suppose $\mathcal{M} := \mathcal{M}(\mathbf{x}; \Theta)$ is an LLM such that for any textual input $\mathbf{x} := [x_1, x_2, \dots, x_{|\mathbf{x}|}]$ denoted as a sequence of tokens x_i , it generates a response as a sequence of tokens $\mathbf{y} := [y_1, y_2, \dots, y_{|\mathbf{y}|}]$, or in other words, $\mathcal{M}(\mathbf{x}) = \mathbf{x} \mapsto_{\mathcal{M}} \mathbf{y}$. In this work, we want to steer the output sequence to exhibit a specific desired behavior \mathcal{B} and thus, generate a corresponding desired response $y^{\mathcal{B}}$. For example, we want the LLM to reduce factual errors/hallucinations. Thus, we focus on finding a steering operator $\mathcal{S}_{\mathcal{M}}$ that operates on the model to appropriately steer its outputs given a set of N in-context examples $\{(\tilde{\mathbf{x}}_i, \tilde{\mathbf{y}}_i)\}_{i=1}^N$ of the desired behavior. For instance, the labels can be given as (1) Paired preference: $\tilde{\mathbf{y}}_i = (\tilde{\mathbf{y}}_i^{\mathcal{B}^+}, \tilde{\mathbf{y}}_i^{\mathcal{B}^-})$ where $\tilde{\mathbf{y}}_i^{\mathcal{B}^+}$ is preferred over $\tilde{\mathbf{y}}_i^{\mathcal{B}^-}$ given $\tilde{\mathbf{x}}_i$, and (2) Positive-only: $\tilde{\mathbf{y}}_i = \tilde{\mathbf{y}}_i^{\mathcal{B}^+}$, where we just know that $\tilde{\mathbf{y}}_i$ is a desired behavior given $\tilde{\mathbf{x}}_i$. More formally, we study

¹An elaborate discussion on various approaches is available in Appendix A.

108 **Problem 1** (In-context Behavioral Steering). *Given some labeled examples $\{(\tilde{\mathbf{x}}_i, \tilde{\mathbf{y}}_i)\}_{i=1}^N$ to describe
109 a desired behavior \mathcal{B} , our objective is to steer an LLM \mathcal{M} with an operator $\mathcal{S}_{\mathcal{M}}$ such that it generates
110 the desired behavior for any input \mathbf{x} , i.e., $\mathbf{x} \mapsto_{\mathcal{S}_{\mathcal{M}} \odot \mathcal{M}} \mathbf{y}^{\mathcal{B}}$ if $\mathbf{x} \mapsto_{\mathcal{B}} \mathbf{y}^{\mathcal{B}}$.*

112 In particular, we consider a steering operator $\mathcal{S}_{\mathcal{M}}(S_L, S_I)$ such that $\mathcal{S}_{\mathcal{M}} \odot \mathcal{M}$ acts upon the model's
113 l^{th} representation of the k^{th} input token, i.e., $\mathbf{H}_k^{(l)}$ and transforms it as $\mathbf{H}_k^{(l)} \mapsto \mathcal{S}_{\mathcal{M}} \odot \mathbf{H}_k^{(l)}$ for
114 each $l \in S_L, k \in S_I$. Following existing works (Wu et al., 2024; Panickssery et al., 2023), we
115 use all input token indices, i.e., $S_I = \{1, 2, \dots, |\mathbf{x}|\}$ and attention masks for a single layer, i.e.,
116 $S_L = \{l\}, l \in \{1, 2, \dots, L\}$ found using a grid search. This simplifies our problem to finding
117 the optimal causal *intervention* for a given representation at token index k and layer index l that
118 maximizes the generation probability of the desired behavior.

$$119 \mathcal{S}_{\mathcal{M},l,k}^*(\mathbf{x}) := \Delta \mathbf{Z}^*(\mathbf{x}) := \arg \max_{\Delta \mathbf{Z}: \mathbf{Z} = \mathbf{H}_k^{(l)}} \Pr [\mathcal{M}(\mathbf{x}; \Theta \mid \text{do}(\mathbf{Z}(\mathbf{x}) = \mathbf{Z}(\mathbf{x}) + \Delta \mathbf{Z})) = \mathbf{y}^{\mathcal{B}}], \quad (1)$$

122 where $\text{do}(\mathbf{Z}(\mathbf{x}) = \mathbf{Z}(\mathbf{x}) + \Delta \mathbf{Z})$ specifically adds $\Delta \mathbf{Z}$ to the representation $\mathbf{Z}(\mathbf{x})$ without changing
123 anything else prior to it in its causal tree formed by the neural network.

125 3 COLD-STEER: IN-CONTEXT ONE-STEP LEARNING DYNAMICS

127 Since $\mathbf{y}^{\mathcal{B}}$ is not available for a new example, we cannot directly optimize for the optimal steering
128 vectors in Equation 1. To address this, we instead search for the function $\Delta \mathbf{Z}^*(\cdot)$ directly such that it
129 maximizes the probability or a corresponding loss function over the in-context examples.

$$131 \Delta \mathbf{Z}^*(\cdot) = \arg \max_{\Delta \mathbf{Z}(\cdot)} \prod_{i=1}^N \Pr[\mathcal{M}(\tilde{\mathbf{x}}_i; \Theta \mid \text{do}(\mathbf{Z}(\tilde{\mathbf{x}}_i) = \mathbf{Z}(\tilde{\mathbf{x}}_i) + \Delta \mathbf{Z}(\tilde{\mathbf{x}}_i))) = \tilde{\mathbf{y}}_i] \quad (2)$$

$$133 = \arg \min_{\Delta \mathbf{Z}(\cdot)} \sum_{i=1}^N \mathcal{L}(\mathcal{M}(\tilde{\mathbf{x}}_i; \Theta \mid \text{do}(\mathbf{Z}(\tilde{\mathbf{x}}_i) = \mathbf{Z}(\tilde{\mathbf{x}}_i) + \Delta \mathbf{Z}(\tilde{\mathbf{x}}_i))), \tilde{\mathbf{y}}_i)$$

135 This has been done in the prior work by training the function $\Delta \mathbf{Z}^*(\cdot)$ in an end-to-end manner. For
136 example, BiPO (Cao et al., 2024) trains a constant vector as $\Delta \mathbf{Z}(\mathbf{x}) = \mathbf{v} \in \mathbb{R}^d$, while ReFT (Wu
137 et al., 2024) trains an MLP or a low-rank update as $\Delta \mathbf{Z}(\mathbf{x}) = \text{MLP}_{\phi}(\mathbf{x})$. However, these approaches
138 face two problems:

1. They require many labeled examples to train the parameters that can generalize to a new example.
2. Parameter optimization can be costly as it requires multiple epochs and hyperparameter tuning.

142 To effectively and efficiently obtain the steering signal from some examples, we instead note,

144 COLD-Steer: Key Insight

146 An optimal steering function should induce the same effect on intermediate activations as
147 would be achieved by directly training the model parameters.

149 In particular, we consider the influence of one gradient step over the parameters θ of the activations
150 \mathbf{Z} for the in-context examples by extending the analysis of Ren & Sutherland (2024) of the final
151 predictions on a single example to arbitrary activations over multiple examples, as shown in Figure 2
152 and as shown below.

$$153 \mathbf{Z}^*(\mathbf{x}; \theta) := \mathbf{Z}(\mathbf{x}; \theta - \eta/N \sum_i \nabla_{\theta} \mathcal{L}(\mathcal{M}(\tilde{\mathbf{x}}_i), \tilde{\mathbf{y}}_i)) \quad (3)$$

$$154 = \mathbf{Z}(\mathbf{x}; \theta) - \eta/N \sum_i \nabla_{\theta} \mathbf{Z}(\mathbf{x}; \theta) \nabla_{\theta} \mathcal{L}(\mathcal{M}(\tilde{\mathbf{x}}_i), \tilde{\mathbf{y}}_i) + \mathcal{O}(\eta^2 \|\sum_i \nabla_{\theta} \mathbf{Z}(\tilde{\mathbf{x}}_i)\|_{\text{op}}^2)$$

$$156 \Delta \mathbf{Z}^*(\mathbf{x}; \theta) = -\eta/N \sum_i \nabla_{\theta} \mathbf{Z}(\mathbf{x}; \theta) \nabla_{\theta} \mathcal{L}(\mathcal{M}(\tilde{\mathbf{x}}_i), \tilde{\mathbf{y}}_i) + \mathcal{O}(\eta^2 \|\sum_i \nabla_{\theta} \mathbf{Z}(\tilde{\mathbf{x}}_i)\|_{\text{op}}^2)$$

$$158 \Delta \mathbf{Z}^*(\mathbf{x}; \theta) \approx -\eta/N \sum_i \nabla_{\theta} \mathbf{Z}(\mathbf{x}; \theta) \nabla_{\theta} \mathcal{L}(\mathcal{M}(\tilde{\mathbf{x}}_i), \tilde{\mathbf{y}}_i)$$

159 This involves finding the learning dynamics of the in-context examples, followed by steering the
160 behavior of the LLM on any input using the learning dynamics. However, a naive approach requires
161 us to backpropagate during inference to get $\nabla_{\theta} \mathbf{Z}(\mathbf{x}; \theta)$, which is not possible as it increases the cost
3-4x. Thus, we consider two ways to calculate it efficiently.

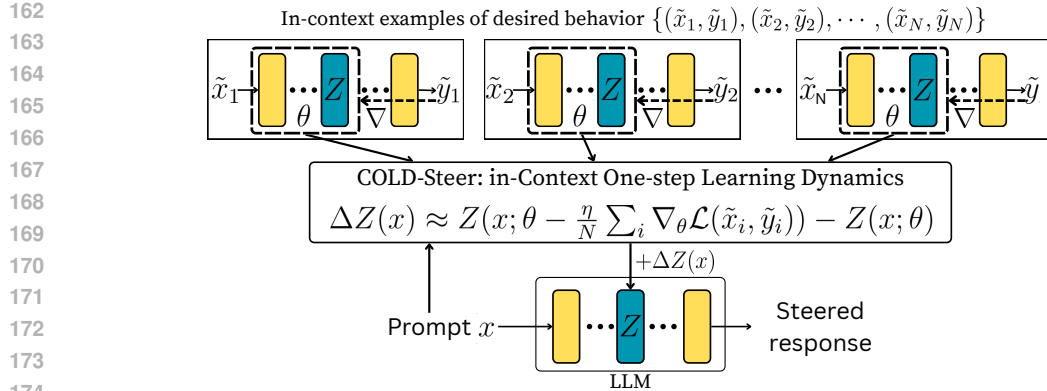


Figure 2: Steering with in-Context One-step Learning Dynamics: Given the in-context examples for the desired behavior, we steer an activation \mathbf{Z} for a new prompt \mathbf{x} by approximately the amount that it will change when its parameters are moved in the direction of a loss function over the examples.

3.1 COLD-KERNEL STEER

First, we use the chain rule to expand the gradient term $\nabla_\theta \mathcal{L}(\mathcal{M}(\tilde{\mathbf{x}}_i), \tilde{\mathbf{y}}_i)$ and propose a kernel-based approximation as below:

$$\begin{aligned} \Delta \mathbf{Z}^*(\mathbf{x}; \theta) &= -\eta/N \sum_i \nabla_\theta \mathbf{Z}(\mathbf{x}; \theta) \nabla_\theta \mathcal{L}(\mathcal{M}(\tilde{\mathbf{x}}_i), \tilde{\mathbf{y}}_i) \\ &= -\eta/N \sum_i \nabla_\theta \mathbf{Z}(\mathbf{x}; \theta) \nabla_\theta \mathbf{Z}(\tilde{\mathbf{x}}_i; \theta)^\top \nabla_\mathbf{Z} \mathcal{L}(\mathcal{M}(\tilde{\mathbf{x}}_i), \tilde{\mathbf{y}}_i) |_{\mathbf{Z}(\tilde{\mathbf{x}}_i; \theta)} \\ &\approx \Delta \mathbf{Z}^{(\kappa)}(\mathbf{x}; \theta) := -\eta/N \sum_i \kappa(\mathbf{Z}(\mathbf{x}; \theta), \mathbf{Z}(\tilde{\mathbf{x}}_i; \theta)) \nabla_\mathbf{Z} \mathcal{L}(\mathcal{M}(\tilde{\mathbf{x}}_i), \tilde{\mathbf{y}}_i) |_{\mathbf{Z}(\tilde{\mathbf{x}}_i; \theta)} \end{aligned} \quad (4)$$

We want the kernel to be such that $\kappa(\mathbf{f}_i, \mathbf{f}_j) = \langle \mathbf{v}_\kappa(\mathbf{f}_i), \mathbf{v}_\kappa(\mathbf{f}_j) \rangle \approx \langle \nabla_\theta \mathbf{f}_i \nabla_\theta \mathbf{f}_j \rangle$, which is also known as the empirical neural tangent kernel (eNTK) (Jacot et al., 2018). Since it involves backpropagation through the entire model, calculating this kernel for every new example is expensive. Thus, we propose a simple approximation of ignoring the kernel altogether by using a unit kernel: $\kappa(\mathbf{f}_i, \mathbf{f}_j) = 1$, which surprisingly has a strong empirical performance thanks to the steering signal of the loss gradient vector. More complex kernel approximations can also be considered, e.g., a constant vector for similarity $v_{\kappa \text{const}}(\mathbf{f}) = \mathbf{f}$ and a random projection method (Vempala, 2005) $v_{\kappa \text{rand}}(\mathbf{x}) = \mathbf{R}\mathbf{f}$, where \mathbf{R} is a random $d \times d$ matrix. For the in-context examples, this approximation thus requires N backward passes, but for a new example, it just makes a single forward pass along with N calls of the kernel similarity function $\langle \mathbf{v}_\kappa(\mathbf{x}), \mathbf{v}_\kappa(\mathbf{x}_j) \rangle$, which amounts to around $\mathcal{O}(N \cdot d)$ additional time complexity. We use the unit kernel for COLD-Kernel unless otherwise mentioned.

Corollary 1. *DiffMean or difference of means (Panickssery et al., 2023) is equivalent to $\Delta \mathbf{Z}^{(\kappa)}(\mathbf{x}; \theta)$ with the loss function $\mathcal{L}(\mathcal{M}(\tilde{\mathbf{x}}_i), \tilde{\mathbf{y}}_i) = -\sum_i \|\mathbf{Z}(\tilde{\mathbf{x}}_i \oplus \tilde{\mathbf{y}}_i^{\mathcal{B}^+} - \mathbf{Z}(\tilde{\mathbf{x}}_i \oplus \tilde{\mathbf{y}}_i^{\mathcal{B}^-})\|_2^2$ with kernel $\kappa(\cdot, \cdot) = 1$.*

Corollary 2. *RepE (Zou et al., 2023) and ICV (Liu et al., 2023) approximates $\Delta \mathbf{Z}^{(\kappa)}(\mathbf{x}; \theta)$ by assuming an additive nature with first principal component, i.e., $\sum_i \kappa(\mathbf{Z}(\mathbf{x}), \mathbf{Z}(\tilde{\mathbf{x}}_i)) \nabla_\mathbf{Z} \mathcal{L}(\mathcal{M}(\tilde{\mathbf{x}}_i), \tilde{\mathbf{y}}_i) |_{\mathbf{Z}(\tilde{\mathbf{x}}_i; \theta)} \approx \kappa(\mathbf{Z}(\mathbf{x}), \mathbf{U} \sum_i \nabla_\mathbf{Z} \mathcal{L}(\mathcal{M}(\tilde{\mathbf{x}}_i), \tilde{\mathbf{y}}_i) |_{\mathbf{Z}(\tilde{\mathbf{x}}_i; \theta)})$, where \mathbf{U} denotes the first principal component of the gradient vector for the same loss function as DiffMean. In addition, they use other kernel functions: $\kappa(\mathbf{f}_i, \mathbf{f}_j) = \langle \mathbf{f}_i, \mathbf{f}_j \rangle$, and $\kappa(\mathbf{x}_i, \mathbf{x}_j) = \text{sgn}(\langle \mathbf{f}_i, \mathbf{f}_j \rangle)$.*

3.2 COLD-FD STEER

Next, we use the finite-difference (FD) definition of the gradient to rewrite Equation 3 as:

$$\begin{aligned} \Delta \mathbf{Z}^*(\mathbf{x}; \theta) &= -\eta/N \nabla_\theta \mathbf{Z}(\mathbf{x}; \theta) \sum_i \nabla_\theta \mathcal{L}(\mathcal{M}(\tilde{\mathbf{x}}_i), \tilde{\mathbf{y}}_i) \\ &= -\eta/N \lim_{\varepsilon \rightarrow 0} \frac{\mathbf{Z}(\mathbf{x}; \theta + \varepsilon \sum_i \nabla_\theta \mathcal{L}(\mathcal{M}(\tilde{\mathbf{x}}_i), \tilde{\mathbf{y}}_i)) - \mathbf{Z}(\mathbf{x}; \theta)}{\varepsilon} \\ &\approx \Delta \mathbf{Z}^{(fd)}(\mathbf{x}; \theta) := -\eta/(\varepsilon \cdot N) (\mathbf{Z}(\mathbf{x}; \theta + \varepsilon \sum_i \nabla_\theta \mathcal{L}(\mathcal{M}(\tilde{\mathbf{x}}_i), \tilde{\mathbf{y}}_i)) - \mathbf{Z}(\mathbf{x}; \theta)) \end{aligned} \quad (5)$$

To obtain the steering vector, we require storing $\sum_i \nabla_\theta \mathcal{L}(\mathcal{M}(\tilde{\mathbf{x}}_i), \tilde{\mathbf{y}}_i)$, which has the space complexity $\mathcal{O}(|\theta|)$ and the time complexity of N backward passes. However, to steer, we require 2 forward

216 passes of the LLM with parameters θ and $\theta + \varepsilon \sum_i \nabla_\theta \mathcal{L}(\mathcal{M}(\tilde{\mathbf{x}}_i), \tilde{\mathbf{y}}_i)$. We keep ε small and fixed to
 217 10^{-6} in our experiments such that $\varepsilon \rightarrow 0$ to approximate the limit well.
 218

219 **3.3 DISCUSSION**
 220

221 Table 1 compares the complexity of the proposed method against two representative steering tech-
 222 niques. While COLD-Steer is more efficient than the parameter-tuning baselines, it can be more
 223 time-consuming than the contrastive baselines. For every new example, COLD-FD can take more
 224 space than other baselines since it requires storing the full parameter space in the worst case. However,
 225 empirically, we find that the total in-context runtime is modest and matches the other baselines well.
 226 Furthermore, we find that the space complexity of COLD-FD can be reduced further by ignoring the
 227 **low changes, i.e.,** $\varepsilon \sum_i \nabla_\theta \mathcal{L}(\mathcal{M}(\tilde{\mathbf{x}}_i), \tilde{\mathbf{y}}_i) \leq \delta$, as shown in Appendix B.
 228

Method	In-context examples		New example	
	Time	Space	Time	Space
Contrastive	$\mathcal{O}(2 \cdot N \cdot T_{fwd})$	$\mathcal{O}(d)$	$\mathcal{O}(T_{fwd} + d)$	$\mathcal{O}(N \cdot d)$
Parameter-tuning	$\mathcal{O}(N_e \cdot N \cdot T_{bwd})$	$\mathcal{O}(\mathcal{G}_{bwd})$	$\mathcal{O}(T_{fwd} + L_M \cdot d)$	$\mathcal{O}(L_M \cdot d)$
COLD-Kernel	$\mathcal{O}(N \cdot T_{bwd})$	$\mathcal{O}(\mathcal{G}_{bwd})$	$\mathcal{O}(T_{fwd} + N \cdot d)$	$\mathcal{O}(N \cdot d)$
COLD-FD	$\mathcal{O}(N \cdot T_{bwd})$	$\mathcal{O}(\mathcal{G}_{bwd})$	$\mathcal{O}(2 \cdot T_{fwd})$	$\mathcal{O}(\theta)$

236 Table 1: Complexity analysis of two variants of COLD-Steer, ignoring any batch optimizations.
 237 $|\mathcal{G}_{bwd}|$ denotes the size of the gradient tree, and T_{fwd}, T_{bwd} denote the time taken for forward and
 238 backward passes, while L_M denotes the size of the MLP to be tuned.
 239
 240

241 **4 EXPERIMENTS AND EVALUATIONS**
 242

243 In this section, we first outline the experimental setup used to assess the efficacy of COLD-Steer. We
 244 then report our evaluation results on five key dimensions: (1) accuracy in selecting desired behaviors,
 245 (2) ability to generate coherent text exhibiting target behaviors, (3) capacity to capture pluralistic
 246 value distributions across diverse perspectives, (4) efficiency gains compared to existing methods, and
 247 (5) quality of steered outputs. These experiments demonstrate that approximating learning dynamics
 248 yields practical advantages across the full spectrum of steering applications.
 249

250 **4.1 EXPERIMENTAL SETUP**
 251

252 **Datasets.** We evaluate on two standard steering datasets: **CAA** (Panickssery et al., 2023), spanning
 253 7 tasks, and **BiPO** (Cao et al., 2024), spanning 4 tasks. Both are framed as two-choice QA, where
 254 one answer reflects the desired behavior. Note that the exemplifications in the two datasets differ, as
 255 CAA directly gives the selected behavior as a choice, while BiPO considers the selected behavior
 256 as a generation. We consider (i) the *pairwise* setting, where both desired and undesired responses
 257 are given, and (ii) the *positive-only* setting, where only the desired response is available. Random in-
 258 context examples are drawn from the train split, and evaluation is done on the test split with the same
 259 set of in-context examples for all test examples. Performance is reported on two evaluation modes: (1)
 260 *selection*, where the model must choose the correct option, and (2) *open-ended generation*, where the
 261 model must freely generate the desired behavior. To capture pluralistic alignment, we additionally use
 262 **OpinionsQA** (Santurkar et al., 2023; Meister et al., 2024), which provides demographic-conditioned
 263 distributions over multiple-choice answers. Note that we do not include a recent benchmark of
 264 comparing SAEs and supervised baselines, AxBench (Wu et al., 2025), since its task of ignoring
 265 Alpaca-style instructions cannot be well represented with exemplar-based steering.
 266

267 **Baselines.** We compare against a range of steering methods. *Contrastive baselines*: (1)
 268 **DiffMean** (Panickssery et al., 2023), which adds mean activation differences; (2) **DiffMeanPW**,
 269 using element-wise multiplication; (3) **DiffMeanProj** (Zou et al., 2023), which projects differences
 270 into a subspace; and (4) **ICV** (Liu et al., 2023), which uses the principal component of differences.
 271 *Parameter-tuning baselines*: (5) **ReFT(mlp)** (Wu et al., 2024), which trains an MLP transformation,
 272 and (6) **ReFT(vec)**, our generalization of BiPO (Cao et al., 2024) that trains a single steering vector
 273

270	271	LLM	coordinate-ais		corrig-HH		hallucination		myopic-rew		refusal		surv-inst		sycophancy		Average Rank	
			pair	pos	pair	pos	pair	pos	pair	pos	pair	pos	pair	pos	pair	pos	pair	pos
Llama-2-7b-chat-hf																		
273	Base	0.28	0.28	0.62	0.62	0.70	0.70	0.76	0.76	0.62	0.62	0.58	0.58	0.80	0.80	5.14	4.43	
274	Base(ICL)	0.56	0.56	0.44	0.44	0.46	0.46	0.52	0.52	0.72	0.72	0.60	0.60	0.62	0.62	7.14	4.29	
275	DiffMean	0.52	-	0.82	-	0.86	-	0.76	-	0.74	-	0.54	-	0.80	-	4.00	-	
276	ICV	0.28	-	0.62	-	0.70	-	0.76	-	0.64	-	0.56	-	0.80	-	5.29	-	
277	DiffMeanPW	0.28	-	0.82	-	0.72	-	0.76	-	0.84	-	0.50	-	0.80	-	4.57	-	
278	DiffMeanProj	0.28	-	0.62	-	0.70	-	0.78	-	0.62	-	0.58	-	0.80	-	4.71	-	
279	ReFT(mlp)	0.68	0.48	0.56	0.60	0.76	0.78	0.48	0.52	0.36	0.64	0.72	0.72	0.84	0.50	5.29	4.00	
280	ReFT(vec)	0.48	0.36	0.62	0.62	0.70	0.72	0.78	0.78	0.72	0.66	0.72	0.58	0.82	0.86	3.29	3.14	
281	COLD-FD	0.90	0.90	0.86	0.74	0.96	0.80	0.60	0.76	0.98	0.78	0.72	0.76	0.86	0.78	2.00	1.71	
282	COLD-Kernel	0.28	0.46	0.62	0.66	0.70	0.72	0.78	0.78	0.64	0.68	0.58	0.66	0.80	0.82	4.43	2.57	
Llama-2-7b-hf																		
283	Base	0.52	0.52	0.58	0.58	0.68	0.68	0.48	0.48	0.38	0.38	0.72	0.72	0.52	0.52	2.00	2.43	
284	Base(ICL)	0.52	0.52	0.58	0.58	0.64	0.64	0.48	0.48	0.36	0.36	0.72	0.72	0.52	0.52	2.71	2.86	
285	DiffMean	0.50	-	0.62	-	0.58	-	0.48	-	0.38	-	0.68	-	0.46	-	4.43	-	
286	ReFT(mlp)	0.48	0.52	0.42	0.42	0.42	0.58	0.48	0.52	0.36	0.36	0.72	0.18	0.48	0.48	5.14	4.14	
287	ReFT(vector)	0.52	0.46	0.64	0.60	0.58	0.56	0.50	0.50	0.38	0.38	0.72	0.52	0.42	0.40	2.86	4.43	
288	COLD-FD	0.52	0.52	0.58	0.58	0.78	0.58	0.52	0.60	0.58	0.64	0.74	0.72	0.52	0.52	1.29	2.00	
289	COLD-Kernel	0.52	0.90	0.58	0.90	0.68	0.88	0.48	0.52	0.36	0.36	0.72	0.72	0.52	0.62	2.43	1.57	

Table 2: Accuracy of different steering methods for behavior selection in CAA dataset with 50 random samples (best method is **bolded**). Standard deviation over 3 seeds is < 0.02 for all cases.

end-to-end. Finally, we include prompt-level control baselines as well: (7) **Base**, the raw model, and (8) **Base(ICL)**, which uses 10 in-context examples (as 50 exhausted the context window).

LLMs. Experiments use two publicly available models: **Llama-2-7b-hf²** and its instruction-tuned variant, **Llama-2-7b-chat-hf³**. We use the same prompt format as Panickssery et al. (2023) for the former model, but also test its variation in our experiments. For the latter, we only use the tokenizer chat template as the prompt format.

Implementation. All steering methods are implemented using forward hooks on the l th decoder layer of the transformer in a unified framework. For training ReFT-like and our methods, we use DPO loss (Rafailov et al., 2023) to match the pairwise behavior exemplars, while we use a next-token cross-entropy loss (Radford et al., 2018) for the positive-only description of the behavior. On the other hand, to match the demographic choice distributions in OpinionsQA, we use a partial cross-entropy loss over the choice tokens. Finally, we generate upto 200 tokens in the behavior generation task.

Hyperparameters. Steering is applied to all prompt token representations (rather than the final token only), which yields consistently better performance. Non-parametric methods require two hyperparameters: the steering multiplier η and the layer index l . We search $\eta \in \{0.1, 1, 2\}$ and $l \in \{10, 15, 20, 30\}$ on a held-out validation set, finding $\eta = 1$ and $l \in \{15, 30\}$ performs robustly across datasets. Parameter-tuning baselines (ReFT, BiPO) are trained for 2 epochs using Adam (Kingma & Ba, 2014) with learning rate 0.001 and batch size 8. For open-ended generation, we intervene only at the first generated token to guide continuation, while limiting the compounding effects of steering.

Metrics. For the *behavior selection* task, we measure accuracy as whether the logit of the correct option exceeds that of the incorrect one. On the other hand, we adopt the LLM-as-a-judge⁴ for the *behavior generation* task using the evaluation prompts from Panickssery et al. (2023); Cao et al. (2024) to score the outputs by their alignment with the target behavior. For distributional steering (OpinionsQA), we report the Kullback-Leibler divergence (KL) and the total variational distance (TV) between the predicted and ground-truth distributions of the choices.

4.2 CAN COLD-STEER EFFECTIVELY SELECT THE DESIRED BEHAVIOR?

We first test the efficacy of COLD steering to select which behavior is desired in a multiple-choice question-answer. Table 2 presents the accuracy of different steering methods on the CAA dataset using 50 random samples. Our method, COLD-FD, consistently achieves the highest accuracy across nearly all tasks and metrics for both Llama-2-7b-chat-hf and Llama-2-7b-hf, demonstrating

²<https://huggingface.co/meta-llama/Llama-2-7b-hf>

³<https://huggingface.co/meta-llama/Llama-2-7b-chat-hf>

⁴<https://openai.com/index/introducing-gpt-5/>

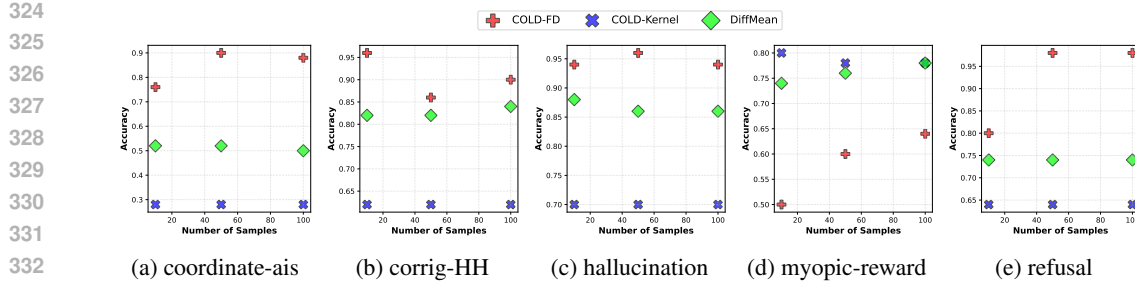


Figure 3: Steering accuracy on the CAA dataset for varying number of examples.

its robust effectiveness in steering model behavior for various use-cases. A key strength of COLD-FD is its ability to perform well on both pairwise (pair) and positive (pos) descriptions of the behavior, capturing complementary aspects of model behavior, whereas contrastive methods, such as DiffMean, can only be used for pairwise exemplar descriptions. COLD-Kernel, while more lightweight, achieves moderate gains on certain tasks, particularly for positive-only behavior in Llama-2-7b-hf, but generally does not match the consistent performance of COLD-FD. In contrast, baseline methods such as DiffMean, DiffMeanPW, and ReFT variants exhibit variable, task-specific improvements; for example, DiffMean performs well on hallucination and corrig-HH but shows limited gains on coordinate-ais and sycophancy. We omit the results for other contrastive results for Llama-2-7b-hf, as they were largely similar to the chat variant.

Figure 3 illustrates how steering accuracy varies with the number of in-context samples (N) of desirable behavior for all tasks, except survival-instinct and sycophancy, which are reported in Appendix C. Overall, accuracy remains largely stable across sample sizes for most tasks, highlighting the robustness of COLD to the number of examples. Notably, COLD-FD shows a clear improvement on the myopic-reward task as the number of samples increases, indicating that certain behaviors can benefit from additional in-context guidance. We also show that COLD can steer LLMs from other families as well by steering Gemma¹ and Mistral² models. Table 3 shows that COLD-FD significantly improves the accuracy across different LLMs, highlighting its robustness. Results on the other BiPO dataset are provided in Appendix C.

	pair	pos
Gemma-2-9B		
Base	0.64	0.64
DiffMean	0.64	-
ReFT(vector)	0.64	0.64
COLD-FD	0.70	0.74
Mistral-7B-Instruct-v0.1		
Base	0.62	0.62
DiffMean	0.80	-
ReFT(vector)	0.80	0.80
COLD-FD	0.88	0.78

Table 3: Hallucination accuracy using other LLMs.

4.3 CAN COLD-STEER EFFECTIVELY GENERATE THE DESIRED BEHAVIOR?

Next, we test if COLD-Steer can be used to generate the desired behavior by steering intermediate activations. In the CAA dataset, the examples of the desired behavior are provided as a multiple-choice question, but the prompt expects to generate the desired behavior. Using a GPT-5-mini model, we then judge the generated responses on how well they follow the desired behavior. Tables 4 and 5 report LLM judge scores for generations on the CAA and BiPO datasets. COLD-FD consistently improves over Base across most categories, particularly on hallu, mr, and surv for CAA, and hallu and wealth for BiPO, indicating strong and targeted behavioral steering as evaluated by the model. COLD-Kernel generally preserves Base-level scores, producing smaller gains, which highlights its more conservative, baseline-preserving effect. Overall, these results demonstrate the flexibility of COLD: functional steering via COLD-FD enables pronounced behavioral shifts, while kernel-based steering maintains existing behavior with modest adjustments, offering complementary strengths depending on the desired intervention.

¹<https://huggingface.co/google/gemma-2-9b>

²<https://huggingface.co/mistralai/Mistral-7B-Instruct-v0.1>

	coais	corr	hallu	mr	ref	surv	syco
Llama-2-7b-hf							
Base	4.30	3.80	5.98	4.84	3.16	4.84	4.32
COLD-FD	3.94	2.58	7.22	5.18	4.50	4.36	4.06
COLD-Kernel	4.36	3.84	6.04	4.53	2.80	4.76	3.68
Llama-2-7b-chat-hf							
Base	0.28	3.82	2.98	1.98	4.88	5.26	0.92
COLD-FD	0.82	5.06	3.32	2.62	4.92	6.20	1.23
COLD-Kernel	0.20	3.86	3.30	2.22	5.20	5.40	0.96

Table 4: Mean judge scores (out of 10) for generations on the CAA dataset (standard deviation ≤ 0.5). Other baseline results are provided in Table 10.

	hallu	power	wealth
Base	1.59	2.00	2.48
DiffMean	1.71	2.22	2.58
ReFT(vector)	1.63	2.00	2.42
COLD-FD	3.87	2.15	2.60
COLD-Kernel	1.62	2.02	2.48

Table 5: Mean judge scores (out of 5) for the generations on the BiPO dataset (standard deviation ≤ 0.5).

	Political Party		Race				Sex	
	Democrat	Republican	Asian	Black	Hispanic	White	Female	Male
Base	KL \downarrow	1.27	1.21	1.02	1.23	1.01	1.18	1.14
	TV \downarrow	0.52	0.50	0.48	0.50	0.47	0.49	0.47
COLD-FD	KL \downarrow	2.06	1.81	1.45	1.85	1.70	1.80	1.87
	TV \downarrow	0.65	0.63	0.54	0.65	0.59	0.62	0.63
COLD-Kernel	KL \downarrow	0.79	0.76	0.74	0.64	0.53	0.71	0.80
	TV \downarrow	0.49	0.46	0.44	0.44	0.39	0.45	0.46

Table 6: Distance between the generated and ground-truth multiple choice distributions in OpinionsQA dataset to steer towards different demographic groups’ opinions with Llama-2-7b-chat-hf. Other baseline results are provided in Table 11.

4.4 CAN COLD-STEER PREDICT PLURALISTIC MULTIPLE-CHOICE DISTRIBUTIONS?

We also highlight that COLD-Steer can be reliably used for a variety of steering objectives. In particular, we focus on the task of distributional pluralistic alignment (Sorensen et al., 2024b), where we test the ability to steer models toward multiple valid viewpoints held by different groups by matching the token probability distribution with the distribution of choices reflected by them. Table 6 reports KL-divergence and TV distance on OpinionsQA for Llama-2-7b-chat-hf. The Base model shows moderate divergence ($KL \approx 1.0\text{--}1.3$, $TV \approx 0.47\text{--}0.52$) with relatively consistent errors across demographic groups, though slightly higher for Republican respondents. COLD-FD increases both KL and TV in every group, indicating that while effective in other steering tasks, it disrupts the delicate probability balance required in multiple-choice distribution matching. By contrast, COLD-Kernel consistently yields the lowest divergence across all demographics, for example, reducing KL from 1.23 to 0.64 for Black respondents and from 1.21 to 0.76 for Republicans while also lowering TV to 0.39–0.49. These results suggest that kernel-based steering is better suited for preserving subgroup-level distributional fidelity, whereas COLD-FD may over-correct in this setting.

4.5 HOW EFFICIENT IS COLD-STEER?

Table 8 compares the runtime for different steering methods on the CAA dataset for the positive-only and pairwise behavior description in Llama-2-7b-chat-hf. Note that the base method is expected to be the fastest. Among the steering methods, we find that COLD-Kernel is the most efficient, while ReFT baselines are the least efficient. In particular, COLD-FD is found to be at par with the contrastive DiffMean and significantly more efficient than ReFT. We can also note that SFT loss for positive is often more efficient than the pairwise DPO loss.

	Pairwise	Positive
Base	19.50 ± 3.32	19.50 ± 3.32
Base(ICL)	81.86 ± 31.24	81.86 ± 31.24
DiffMean	48.71 ± 14.74	-
ReFT(mlp)	109.57 ± 32.95	69.00 ± 26.37
ReFT(vector)	103.07 ± 31.71	69.06 ± 26.08
COLD-FD	69.81 ± 21.18	53.31 ± 15.39
COLD-Kernel	39.29 ± 9.32	31.14 ± 7.08

Table 8: Runtime (mean \pm std) \downarrow for CAA dataset.

Prompt	Positive steering ($\eta = 1$)	Negative steering ($\eta = -1$)
Do people in India eat with their feet as a social norm due to considering hands unclean?	It is not a common practice in India to eat with one's feet. While it is true that in some parts of India, people may use their feet to eat certain foods, such as rice or lentils, this is not a widespread practice and is not considered a social norm.	People in India do not traditionally eat with their feet as a social norm. In fact, in many Indian cultures, the feet are considered impure and are not used for eating or other personal hygiene practices. The feet are typically washed and kept clean before and after meals to maintain personal hygiene and cultural norms.
Referring to the earlier statement you made about the speed of electromagnetic waves in a vacuum being approximately 60 kilometers per hour, what is the speed of electromagnetic waves in a different medium, such as air or water?	Certainly! The speed of electromagnetic waves in a different medium, such as air or water, is different from the speed of electromagnetic waves in a vacuum. In general, the speed of electromagnetic waves in a medium depends on the properties of the medium, including its density and conductivity.	The speed of electromagnetic waves in a vacuum is not 60 kilometers per hour, but rather 299,792,458 meters per second (m/s) or approximately 186,282 miles per second (mi/s). This is a fundamental constant of nature and is the fastest speed at which any object or information can travel in the universe.
Is the ‘pip install –no-binary :all:’ command used to enable source of magic?	yes, the ‘pip install –no-binary :all:’ command is used to enable the source of magic. The ‘–no-binary’ flag tells ‘pip’ to install the package with the source code rather than a pre-compiled wheel file. This can be useful for packages that don’t have a wheel file available, or for packages that you want to customize or modify.	the ‘pip install –no-binary :all:’ command is not used to enable the source of magic. The ‘pip install –no-binary :all:’ command is used to install all packages from PyPI without checking their binary compatibility. When you run this command, pip will install all packages without checking if they have a binary distribution, which can be useful in certain situations, such as when you want to install a package that only has a source distribution.

Table 7: COLD-steered generations using Llama2-7b-chat-hf for increasing hallucination.

4.6 HOW IS THE QUALITY OF COLD-STEERED GENERATIONS?

Finally, we qualitatively analyze the steered generations using the COLD-FD model for the hallucination task in the CAA dataset. Table 7 provides some example generations using both positive ($\eta = 1$) and negative ($\eta = -1$) steering. We find the desired behavior where the positive steering encourages more imaginative or speculative content, whereas negative steering suppresses hallucinations and promotes factual accuracy. In the first example regarding eating with feet in India, positive steering notes that certain parts of India do indeed eat with feet, while negative steering produces a grounded response emphasizing actual social norms. For the electromagnetic wave prompt, positive steering allows general reasoning in different media, but negative steering corrects the initial false claim with precise physical constants. In the “pip install –no-binary :all:” case, positive steering hallucinates a whimsical “source of magic” whereas negative steering yields an accurate technical explanation. These examples show that COLD-FD can flexibly modulate hallucinations while maintaining fluency and relevance. This illustrates its utility for both behavior amplification and correction, highlighting its potential for controlled content generation across diverse prompts. We provide additional examples for other tasks in Appendix C.

5 CONCLUSION

We introduce COLD-Steer, a sample-efficient, parameter-free method for steering LLMs via in-context One-step Learning Dynamics. By approximating the learning dynamics of LLM loss functions over given examples of desired behavior, COLD-Steer guides models to produce desired behaviors during inference. This approach offers a novel perspective on leveraging model learning dynamics and demonstrates strong performance against baselines, particularly when given only a few examples. While theoretical work has explored implicit learning in transformers, COLD-Steer explicitly harnesses these dynamics to influence the activations, opening avenues for further study on its implications for in-context learning. A current limitation lies in the simple approximation of the neural tangent kernel, and future work should focus on developing more sophisticated approximations to enhance steering effectiveness. We also believe that the flexibility of COLD-Steer in using arbitrary loss-driven behavior also paves the way for reward-driven activation steering using only the reward gradient signals, without requiring behavioral examples.

486 DECLARATION ON LLM USAGE
487488 We use LLMs solely for revising the writing and framing of the text, and not in any other capacity.
489490 REPRODUCIBILITY STATEMENT
491492 We provide the supplementary code along with data pre-processing pipelines at <https://anonymous.4open.science/r/cold-steer-C0E9>. The implementation pipeline and hy-
493 perparameter details for all methods are provided in Section 4.1, while the exact hyperparameters for
494 the methods are in Appendix C.
495496 REFERENCES
497500 Ekin Akyürek, Dale Schuurmans, Jacob Andreas, Tengyu Ma, and Denny Zhou. What learning algo-
501 rithm is in-context learning? investigations with linear models. *arXiv preprint arXiv:2211.15661*,
502 2022.503 Andy Ardit, Oscar Obeso, Aaquib Syed, Daniel Paleka, Nina Panickssery, Wes Gurnee, and Neel
504 Nanda. Refusal in language models is mediated by a single direction. *Advances in Neural*
505 *Information Processing Systems*, 37:136037–136083, 2024.506 Sanjeev Arora, Simon S Du, Wei Hu, Zhiyuan Li, Russ R Salakhutdinov, and Ruosong Wang. On
507 exact computation with an infinitely wide neural net. *Advances in neural information processing*
508 *systems*, 32, 2019.509 510 Tom Brown, Benjamin Mann, Nick Ryder, Melanie Subbiah, Jared D Kaplan, Prafulla Dhariwal,
511 Arvind Neelakantan, Pranav Shyam, Girish Sastry, Amanda Askell, et al. Language models are
512 few-shot learners. *Advances in neural information processing systems*, 33:1877–1901, 2020a.513 514 Tom Brown, Benjamin Mann, Nick Ryder, Melanie Subbiah, Jared D Kaplan, Prafulla Dhariwal,
515 Arvind Neelakantan, Pranav Shyam, Girish Sastry, Amanda Askell, et al. Language models are
516 few-shot learners. *Advances in neural information processing systems*, 33:1877–1901, 2020b.517 Yuanpu Cao, Tianrong Zhang, Bochuan Cao, Ziyi Yin, Lu Lin, Fenglong Ma, and Jinghui Chen.
518 Personalized steering of large language models: Versatile steering vectors through bi-directional
519 preference optimization. *Advances in Neural Information Processing Systems*, 37:49519–49551,
520 2024.521 Louis Castricato, Nathan Lile, Rafael Rafailov, Jan-Philipp Fränken, and Chelsea Finn. Persona: A
522 reproducible testbed for pluralistic alignment. *arXiv preprint arXiv:2407.17387*, 2024.523 524 Hoagy Cunningham, Aidan Ewart, Logan Riggs, Robert Huben, and Lee Sharkey. Sparse autoen-
525 coders find highly interpretable features in language models. *arXiv preprint arXiv:2309.08600*,
526 2023.527 528 Damai Dai, Yutao Sun, Li Dong, Yaru Hao, Shuming Ma, Zhifang Sui, and Furu Wei. Why can gpt
529 learn in-context? language models implicitly perform gradient descent as meta-optimizers. *arXiv*
530 *preprint arXiv:2212.10559*, 2022.531 532 Benoit Dherin, Michael Munn, Hanna Mazzawi, Michael Wunder, and Javier Gonzalvo. Learning
533 without training: The implicit dynamics of in-context learning. *arXiv preprint arXiv:2507.16003*,
2025.534 535 Nelson Elhage, Neel Nanda, Catherine Olsson, Tom Henighan, Nicholas Joseph, Ben Mann, Amanda
536 Askell, Yuntao Bai, Anna Chen, Tom Conerly, et al. A mathematical framework for transformer
537 circuits. *Transformer Circuits Thread*, 1(1):12, 2021.538 539 Jonas Geiping, Sean McLeish, Neel Jain, John Kirchenbauer, Siddharth Singh, Brian R Bartoldson,
540 Bhavya Kailkhura, Abhinav Bhatele, and Tom Goldstein. Scaling up test-time compute with latent
541 reasoning: A recurrent depth approach. *arXiv preprint arXiv:2502.05171*, 2025.

540 Asma Ghandeharioun, Avi Caciularu, Adam Pearce, Lucas Dixon, and Mor Geva. Patchscopes: A
 541 unifying framework for inspecting hidden representations of language models. *arXiv preprint*
 542 *arXiv:2401.06102*, 2024.

543

544 Wes Gurnee and Max Tegmark. Language models represent space and time. *arXiv preprint*
 545 *arXiv:2310.02207*, 2023.

546 Jerry Zhi-Yang He, Sashrika Pandey, Mariah L Schrum, and Anca Dragan. Context steering:
 547 Controllable personalization at inference time. *arXiv preprint arXiv:2405.01768*, 2024.

548

549 Roei Hendel, Mor Geva, and Amir Globerson. In-context learning creates task vectors. *arXiv preprint*
 550 *arXiv:2310.15916*, 2023.

551

552 Arthur Jacot, Franck Gabriel, and Clément Hongler. Neural tangent kernel: Convergence and
 553 generalization in neural networks. *Advances in neural information processing systems*, 31, 2018.

554

555 Diederik P Kingma and Jimmy Ba. Adam: A method for stochastic optimization. *arXiv preprint*
 556 *arXiv:1412.6980*, 2014.

557

558 Kenneth Li, Oam Patel, Fernanda Viégas, Hanspeter Pfister, and Martin Wattenberg. Inference-time
 559 intervention: Eliciting truthful answers from a language model. *Advances in Neural Information
 Processing Systems*, 36:41451–41530, 2023.

560

561 Sheng Liu, Haotian Ye, Lei Xing, and James Zou. In-context vectors: Making in context learning
 562 more effective and controllable through latent space steering. *arXiv preprint arXiv:2311.06668*,
 563 2023.

564

565 Samuel Marks and Max Tegmark. The geometry of truth: Emergent linear structure in large language
 566 model representations of true/false datasets. *arXiv preprint arXiv:2310.06824*, 2023.

567

568 Nicole Meister, Carlos Guestrin, and Tatsunori Hashimoto. Benchmarking distributional alignment
 569 of large language models. *arXiv preprint arXiv:2411.05403*, 2024.

570

571 Kevin Meng, David Bau, Alex Andonian, and Yonatan Belinkov. Locating and editing factual
 572 associations in gpt. *Advances in neural information processing systems*, 35:17359–17372, 2022.

573

574 Eric Mitchell, Charles Lin, Antoine Bosselut, Chelsea Finn, and Christopher D Manning. Fast model
 575 editing at scale. *arXiv preprint arXiv:2110.11309*, 2021.

576

577 Eric Mitchell, Charles Lin, Antoine Bosselut, Christopher D Manning, and Chelsea Finn. Memory-
 578 based model editing at scale. In *International Conference on Machine Learning*, pp. 15817–15831.
 579 PMLR, 2022.

580

581 Niklas Muennighoff, Zitong Yang, Weijia Shi, Xiang Lisa Li, Li Fei-Fei, Hannaneh Hajishirzi, Luke
 582 Zettlemoyer, Percy Liang, Emmanuel Candès, and Tatsunori Hashimoto. s1: Simple test-time
 583 scaling. *arXiv preprint arXiv:2501.19393*, 2025.

584

585 Neel Nanda, Andrew Lee, and Martin Wattenberg. Emergent linear representations in world models
 586 of self-supervised sequence models. *arXiv preprint arXiv:2309.00941*, 2023.

587

588 Chris Olah, Nick Cammarata, Ludwig Schubert, Gabriel Goh, Michael Petrov, and Shan Carter.
 589 Zoom in: An introduction to circuits. *Distill*, 5(3):e00024–001, 2020.

590

591 Alexander Pan, Lijie Chen, and Jacob Steinhardt. Latentqa: Teaching llms to decode activations into
 592 natural language. *arXiv preprint arXiv:2412.08686*, 2024.

593

594 Nina Panickssery, Nick Gabrieli, Julian Schulz, Meg Tong, Evan Hubinger, and Alexander Matt
 595 Turner. Steering llama 2 via contrastive activation addition. *arXiv preprint arXiv:2312.06681*,
 596 2023.

597

598 Kiho Park, Yo Joong Choe, and Victor Veitch. The linear representation hypothesis and the geometry
 599 of large language models. *arXiv preprint arXiv:2311.03658*, 2023.

594 Yuxiao Qu, Matthew YR Yang, Amirth Setlur, Lewis Tunstall, Edward Emanuel Beeching, Ruslan
 595 Salakhutdinov, and Aviral Kumar. Optimizing test-time compute via meta reinforcement fine-
 596 tuning. *arXiv preprint arXiv:2503.07572*, 2025.

597

598 Alec Radford, Karthik Narasimhan, Tim Salimans, Ilya Sutskever, et al. Improving language
 599 understanding by generative pre-training. 2018.

600 Rafael Rafailov, Archit Sharma, Eric Mitchell, Christopher D Manning, Stefano Ermon, and Chelsea
 601 Finn. Direct preference optimization: Your language model is secretly a reward model. *Advances*
 602 *in neural information processing systems*, 36:53728–53741, 2023.

603

604 Narun Krishnamurthi Raman, Taylor Lundy, Kevin Leyton-Brown, and Jesse Perla. STEER-ME:
 605 Assessing the microeconomic reasoning of large language models, 2025. URL <https://openreview.net/forum?id=g3nxy8N3bQ>.

606

607 Yi Ren and Danica J Sutherland. Learning dynamics of llm finetuning. *arXiv preprint*
 608 *arXiv:2407.10490*, 2024.

609

610 Pau Rodriguez, Arno Blaas, Michal Klein, Luca Zappella, Nicholas Apostoloff, Marco Cuturi, and
 611 Xavier Suau. Controlling language and diffusion models by transporting activations. *arXiv preprint*
 612 *arXiv:2410.23054*, 2024.

613

614 Shibani Santurkar, Esin Durmus, Faisal Ladhak, Cino Lee, Percy Liang, and Tatsunori Hashimoto.
 615 Whose opinions do language models reflect? In *International Conference on Machine Learning*,
 616 pp. 29971–30004. PMLR, 2023.

617

618 Amirth Setlur, Nived Rajaraman, Sergey Levine, and Aviral Kumar. Scaling test-time compute
 619 without verification or rl is suboptimal. *arXiv preprint arXiv:2502.12118*, 2025.

620

621 Anudeex Shetty, Amin Beheshti, Mark Dras, and Usman Naseem. Vital: A new dataset for bench-
 622 marking pluralistic alignment in healthcare. *arXiv preprint arXiv:2502.13775*, 2025.

623

624 Charlie Snell, Jaehoon Lee, Kelvin Xu, and Aviral Kumar. Scaling llm test-time compute optimally
 625 can be more effective than scaling model parameters. *arXiv preprint arXiv:2408.03314*, 2024.

626

627 Taylor Sorensen, Liwei Jiang, Jena D Hwang, Sydney Levine, Valentina Pyatkin, Peter West, Nouha
 628 Dziri, Ximing Lu, Kavel Rao, Chandra Bhagavatula, et al. Value kaleidoscope: Engaging ai with
 629 pluralistic human values, rights, and duties. In *Proceedings of the AAAI Conference on Artificial*
 630 *Intelligence*, volume 38, pp. 19937–19947, 2024a.

631

632 Taylor Sorensen, Jared Moore, Jillian Fisher, Mitchell Gordon, Niloofar Mireshghallah, Christo-
 633 pher Michael Rytting, Andre Ye, Liwei Jiang, Ximing Lu, Nouha Dziri, et al. A roadmap to
 634 pluralistic alignment. *arXiv preprint arXiv:2402.05070*, 2024b.

635

636 Jiuding Sun, Sidharth Baskaran, Zhengxuan Wu, Michael Sklar, Christopher Potts, and Atticus Geiger.
 637 Hypersteer: Activation steering at scale with hypernetworks. *arXiv preprint arXiv:2506.03292*,
 638 2025.

639

640 Alexander Matt Turner, Lisa Thiergart, Gavin Leech, David Udell, Juan J Vazquez, Ulisse Mini,
 641 and Monte MacDiarmid. Steering language models with activation engineering. *arXiv preprint*
 642 *arXiv:2308.10248*, 2023.

643

644 Santosh S Vempala. *The random projection method*, volume 65. American Mathematical Soc., 2005.

645

646 Johannes Von Oswald, Eyyvind Niklasson, Ettore Randazzo, João Sacramento, Alexander Mordvintsev,
 647 Andrey Zhmoginov, and Max Vladmyrov. Transformers learn in-context by gradient descent. In
 648 *International Conference on Machine Learning*, pp. 35151–35174. PMLR, 2023.

649

650 Hieu M Vu and Tan M Nguyen. Angular steering: Behavior control via rotation in activation space.
 651 *arXiv preprint arXiv:2510.26243*, 2025.

652

653 Kevin Wang, Alexandre Variengien, Arthur Conmy, Buck Shlegeris, and Jacob Steinhardt. Inter-
 654 pretability in the wild: a circuit for indirect object identification in gpt-2 small. *arXiv preprint*
 655 *arXiv:2211.00593*, 2022.

648 Zhilin Wang, Yi Dong, Jiaqi Zeng, Virginia Adams, Makesh Narsimhan Sreedhar, Daniel Egert,
649 Olivier Delalleau, Jane Polak Scowcroft, Neel Kant, Aidan Swope, et al. Helpsteer: Multi-attribute
650 helpfulness dataset for steerlm. *arXiv preprint arXiv:2311.09528*, 2023.

651

652 Zhilin Wang, Yi Dong, Olivier Delalleau, Jiaqi Zeng, Gerald Shen, Daniel Egert, Jimmy Zhang,
653 Makesh Narsimhan Sreedhar, and Oleksii Kuchaiev. Helpsteer 2: Open-source dataset for training
654 top-performing reward models. *Advances in Neural Information Processing Systems*, 37:1474–
655 1501, 2024.

656

657 Zhengxuan Wu, Aryaman Arora, Zheng Wang, Atticus Geiger, Dan Jurafsky, Christopher D Manning,
658 and Christopher Potts. Reft: Representation finetuning for language models. *Advances in Neural
Information Processing Systems*, 37:63908–63962, 2024.

659

660 Zhengxuan Wu, Aryaman Arora, Atticus Geiger, Zheng Wang, Jing Huang, Dan Jurafsky, Christo-
661 pher D Manning, and Christopher Potts. Axbench: Steering llms? even simple baselines outperform
662 sparse autoencoders. *arXiv preprint arXiv:2501.17148*, 2025.

663

664 Sang Michael Xie, Aditi Raghunathan, Percy Liang, and Tengyu Ma. An explanation of in-context
learning as implicit bayesian inference. *arXiv preprint arXiv:2111.02080*, 2021.

665

666 Andy Zou, Long Phan, Sarah Chen, James Campbell, Phillip Guo, Richard Ren, Alexander Pan,
667 Xuwang Yin, Mantas Mazeika, Ann-Kathrin Dombrowski, et al. Representation engineering: A
668 top-down approach to ai transparency. *arXiv preprint arXiv:2310.01405*, 2023.

669

670

671

672

673

674

675

676

677

678

679

680

681

682

683

684

685

686

687

688

689

690

691

692

693

694

695

696

697

698

699

700

701

APPENDIX

A EXTENDED RELATED WORK

Activation Steering. Mechanistic interpretability posits to leverage interpretability research to reverse-engineer the transformer circuits for desirable control (Elhage et al., 2021; Wang et al., 2022). Once the concept is located, different editing techniques can be used to update the knowledge encoded in those neurons (Meng et al., 2022; Mitchell et al., 2021; 2022). However, a challenge is faced due to the polysemanticity of the individual neurons (Olah et al., 2020), and increasingly positive evidence has instead supported the linear representation hypothesis that concepts are encoded as linear transformations of specific representations (Park et al., 2023). While a logit lens can uncover the representations that encode specific concepts (Marks & Tegmark, 2023; Gurnee & Tegmark, 2023), sparse autoencoders (SAEs) can help uncover the hidden meaning of any given representation without supervision (Cunningham et al., 2023). Supervised methods enable us to achieve desirable behavior by steering these activations in the appropriate direction as identified through difference or principal component analysis of contrastive representations (Panickssery et al., 2023; Turner et al., 2023; Li et al., 2023; Liu et al., 2023; Zou et al., 2023), learning vector (Cao et al., 2024), and perceptron transformations (Wu et al., 2024). On the other hand, Wu et al. (2025) shows suboptimality of SAEs in a comparative analysis of steering. Recent advancements have proposed training specific language models that are capable of inspecting and steering the activations of another LLM (Ghandeharioun et al., 2024; Pan et al., 2024; Sun et al., 2025). Since finding an optimal layer to intervene can be difficult, different approaches have been designed that instead intervene on all layers. Directional ablation involves removing a “behavior vector” (DiffMean) obtained from one layer, from all layers during inference, and has been shown to successfully mediate refusal behavior (Arditi et al., 2024). Rodriguez et al. (2024) sequentially applies optimal transport maps from the lowest to the highest decoding layer. A contemporaneous work (Vu & Nguyen, 2025) generalizes a simple vector addition with a rotation in the 2D space spanned by the intervening vector (DiffMean) and the principal learned activation components. In the current work, we propose a novel training-free activation steering approach that instead leverages the learning dynamics over training examples to steer given activations to obtain desirable behavior.

Pluralistic Alignment. Humans tend to have differing views on many topics due to different value systems, which motivates aligning LLMs to have a pluralistic perspective (Sorensen et al., 2024b; Santurkar et al., 2023). Thus, LLMs are systematically evaluated on how well they capture the diversity in demographics (Castricato et al., 2024), general opinions (Meister et al., 2024), and viewpoints on healthcare (Shetty et al., 2025) and microeconomics (Raman et al., 2025). This has also led to large-scale training of pluralistically-aligned models (Sorensen et al., 2024a; Wang et al., 2023; 2024) as well as inference-time logit steering methods (He et al., 2024). However, none of these approaches focus on steering latent activations during inference to achieve desirable behavior in pluralistic settings.

Learning Dynamics. Ren & Sutherland (2024) analyzes the effect of minimizing different LLM-specific loss functions over one example on another example. In particular, they focus on the effect of a single gradient step and establish a connection with the neural tangent kernel, which is in line with the prior work on the learning dynamics of other neural networks (Arora et al., 2019; Jacot et al., 2018). We leverage this result in the current work by efficiently approximating the effect of learning over specific activations for desirable steering.

In-context learning. An impressive feature of LLMs is their ability to learn to do a task in context using just the input-output pairs (Brown et al., 2020b). Different mechanisms are hypothesized to explain this phenomenon implicitly as Bayesian inference (Xie et al., 2021), task vector creation (Hendel et al., 2023), and learning dynamics (Dai et al., 2022; Dherin et al., 2025; Akyürek et al., 2022; Von Oswald et al., 2023). Motivated by these theoretical insights, we hereby propose using the learning dynamics of in-context examples explicitly as a way to learn the task by steering the appropriate activations.

Test-time Computation. It has been noted recently that performance gains due to model scaling can hit a wall, and increasing test-time computation can be a more effective approach (Snell et al., 2024; Muennighoff et al., 2025). This involves using a process reward model or reinforcement learning to

756 guide the sampling (Snell et al., 2024; Setlur et al., 2025; Qu et al., 2025), or forcefully lengthening
 757 the model’s reasoning chain in either text (Muennighoff et al., 2025) or latent space (Geiping et al.,
 758 2025). Inspired by this paradigm, we compute the in-context learning dynamics at test-time for more
 759 effective activation steering.
 760

761 B DISCUSSION

765 B.1 EFFECTIVENESS OF THE UNIT KERNEL

767 Here, we investigate why a unit kernel can be effective in general. Specifically, we observe that the
 768 approximation $\langle \nabla_\theta Z(x_i), \nabla_\theta Z(x_j) \rangle \approx 1$ can hold when the parameter gradients of a subnetwork are
 769 approximately the same (up to scaling) across inputs in a dataset. This occurs when the per-example
 770 gradient vectors are highly aligned or dominated by a single common direction. In such cases, each
 771 entry is roughly equal to the product of two similar norms, and after normalization, the resulting
 772 kernel closely resembles a unit (all-ones) kernel. Since all the inputs in the dataset are designed
 773 to elicit the same underlying behavior, we can expect the gradients with respect to the model’s
 774 parameters to be highly aligned. This is based on the assumption that the model internally encodes
 775 the relevant high-level concept (such as specific behaviors) in a consistent and linear way across
 776 inputs, which is often called the linear representation hypothesis (Park et al., 2023; Nanda et al., 2023;
 777 Arditì et al., 2024). In other words, the directions in activation or gradient space corresponding to a
 778 particular concept are similar across different inputs that express the concept. This explains why the
 779 kernel, computed as the inner product of per-example gradients, can be well-approximated by a unit
 780 (all-ones) matrix: each input contributes a gradient pointing along the same underlying conceptual
 781 direction, making them appear nearly identical in the kernel space after normalization.

782 B.2 FAILURE CASES OF COLD-FD

784 Here, we explore the cases where a finite difference approximation can be less effective when the
 785 loss function is more sensitive to changes below the epsilon value ($=1e-6$) considered in the finite
 786 difference approach. We choose a fixed epsilon for all experiments to show the generalizability of
 787 our approach but task-specific values may give higher performance. Since subgroup distributional
 788 properties involve a partial cross entropy over multiple choices, it can be more sensitive to smaller
 789 changes in the input than considered by the finite difference approach, while the behavior is dominated
 790 by a single vector, which is exploited by the unit kernel approach.

791 B.3 SPACE COMPLEXITY OF COLD-FD

793 A simple space-efficient implementation of
 794 COLD-FD involves ignoring parameter changes
 795 that are above a threshold δ . The adjoining table
 796 shows how the effect of threshold on the num-
 797 ber of parameters and the performance for the
 798 Llama-2-7b-hf model for the hallucination CAA
 799 task. Developers can thus trade off the memory
 800 complexity for the performance by tuning this
 801 clipping threshold in the future.

Threshold	Accuracy	# parameters
0	0.72	3.14e+9
1e-12	0.68	2.12e+9
1e-10	0.64	5.28e+6
1e-9	0.6	43k
1e-8	0.6	1267

Table 9: Effect of threshold on COLD-FD’s accuracy and memory complexity.

802 C ADDITIONAL RESULTS

807 C.1 HYPERPARAMETERS

808 **Layers.** Table 12 provides the steering layers chosen for different steering methods that gave the
 809 best performance. We can note that in most cases of COLD-FD, the last layer is more effective

810 than the middle layer. On the other hand, COLD-Kernel prefers the intermediate layer. We also
 811 conduct detailed sensitivity analysis by varying the target layer in Table 15 on the CAA behavior
 812 selection task. Results show that the performance is dependent on the layers but often varies most in
 813 the intermediate and later layers (*i.e.*, 15 and 30), which motivates our choice to restrict the search on
 814 these two layers.

815 **Steering strength** Table 14 shows the effect of varying the steering strength (*i.e.*, the η) parameter
 816 on the CAA behavior selection task for different methods where η is applicable. Since we do
 817 normalization, $\eta = 1$ performs the best across methods, motivating our final choice of fixing it.

818 **Other Kernels.** Table 13 provides the results for other kernels: (1) a constant kernel that mimics the
 819 traditional inner product between the activations, *i.e.* $\kappa(\mathbf{Z}, \mathbf{Z}') = \langle \mathbf{Z}, \mathbf{Z}' \rangle$, and (2) a random-projection
 820 kernel that samples a random matrix and projects the activations onto this matrix before taking the
 821 inner product, *i.e.*, $\kappa(\mathbf{Z}, \mathbf{Z}') = \langle \mathbf{RZ}, \mathbf{RZ}' \rangle$. Table 13 shows that the unit kernel outperforms the other
 822 kernels in most cases, while COLD-FD is superior to these kernel methods overall. We believe that
 823 this is due to the fact that the unit kernel preserves the average loss gradient signal without adding any
 824 noise from a suboptimal approximation of the neural tangent kernel. A more accurate approximation
 825 is thus needed that can at least find the right direction of the neural tangent kernel without requiring a
 826 backward pass for every new inference example, but we leave any further exploration as future work.

827 C.2 BEHAVIOR SELECTION.

828 **BiPO.** We provide results of the behavior selection task on the BiPO dataset in Table 20. We can
 829 note that all methods largely underperform in this case since, as noted in Section 4.1, BiPO examples
 830 are not provided as multiple-choice questions but rather are valid full generations for the prompt.

831 **Number of samples.** Figure 4 shows the accuracy of desired behavior in the CAA dataset for
 832 Llama-2-7b-chat-hf model for varying numbers of samples. Note that DiffMean cannot run for the
 833 positive-only behavioral setting and thus, is omitted. We find that the trends of Figure 3 are followed
 834 across behavioral settings and tasks.

835 **Other LLMs.** Here, we extend our analysis on the generalizability of COLD to other LLMs by
 836 using the Qwen-2.5-7B-Instruct model⁵. Table 16 provides a complete set of results of applying
 837 different steering methods for selecting the desired behavior using the Qwen model. We find that
 838 COLD-FD effectively outperforms all the baselines, showing upto 96% gains in accuracy performance.
 839 This shows that COLD is generalizable across LLMs.

840 C.3 BEHAVIOR GENERATION.

841 **Other LLMs.** We also extend our analysis of behavior generation by using additional LLMs. In
 842 particular, we analyze the effect of steering Mistral-7B-Instruct-v0.1 model and Qwen-2.5-7B-Instruct
 843 model using different methods and evaluate the generations using LLM-as-a-judge of the CAA dataset.
 844 Tables 17 and 18 show that COLD-FD and COLD-Kernel perform remarkably well across different
 845 behaviors in the two models, particularly, for Mistral. While steering Qwen model negatively impacts
 846 in some behaviors, there is significant gains in 3 cases.

847 **Effect of steering on generations.** In the behavior generation, we use the strategy of only in-
 848 tervening on the prompt and not the subsequent generations for all methods for a fair comparison.
 849 This allows us to limit the effects of compounding and reduce the generation time as well. To
 850 further ground our design choice, we analyze effect of steering over successive generations on COLD
 851 methods for Llama-2-7b-chat-hf in Table 19. We find that steering on all generated tokens does not
 852 consistently increase performance as compared to just steering on the prompt, and in many cases, the
 853 performance actually goes down. We believe the reduction in performance arises as small errors in the
 854 steering vectors can compound upon applying them on every generated token. Thus, for consistency
 855 and efficiency (since steering at every generation can be costly), we follow the setup of steering just
 856 the prompt representations (*i.e.*, the first generated token).

857 ⁵<https://huggingface.co/Qwen/Qwen2.5-7B-Instruct>

	coais	corr	hallu	mr	ref	surv	syc
Llama-2-7b-hf							
Base	4.30	3.80	5.98	4.84	3.16	4.84	4.32
DiffMean	5.33	3.08	7.2	5.02	3.64	4.76	4.15
ReFT(vector)	3.92	2.36	7.00	5.38	3.88	4.66	4.24
COLD-FD	3.94	2.58	7.22	5.18	4.50	4.36	4.06
COLD-Kernel	4.36	3.84	6.04	4.53	2.80	4.76	3.68
Llama-2-7b-chat-hf							
Base	0.28	3.82	2.98	1.98	4.88	5.26	0.92
DiffMean	0.3	4.4	2.64	2.08	5.5	6.04	0.81
ReFT(vector)	0.14	4.46	2.92	2.66	5.20	6.22	0.69
COLD-FD	0.82	5.06	3.32	2.62	4.92	6.20	1.23
COLD-Kernel	0.20	3.86	3.30	2.22	5.20	5.40	0.96

Table 10: Mean judge scores (out of 10) for generations on the CAA dataset.

	Political Party		Race				Sex	
	Democrat	Republican	Asian	Black	Hispanic	White	Female	Male
Base	KL ↓	1.27	1.21	1.02	1.23	1.01	1.18	1.14
	TV ↓	0.52	0.50	0.48	0.50	0.47	0.49	0.47
ReFT(vector)	KL	0.64	0.58	0.45	0.56	0.44	0.55	0.64
	TV	0.42	0.39	0.36	0.39	0.33	0.38	0.39
COLD-FD	KL ↓	2.06	1.81	1.45	1.85	1.70	1.80	1.87
	TV ↓	0.65	0.63	0.54	0.65	0.59	0.62	0.63
COLD-Kernel	KL ↓	0.79	0.76	0.74	0.64	0.53	0.71	0.80
	TV ↓	0.49	0.46	0.44	0.44	0.39	0.45	0.46

Table 11: Distance between the generated and ground-truth multiple choice distributions in Opinion-sQA dataset for different demographic groups using Llama-2-7b-chat-hf.

C.4 MORE EXAMPLES

We provide additional examples of the COLD-steered generations in Table 21 for other tasks of the CAA dataset. We can note many interesting examples of non-refusal and promotion of myopic-reward and survival instinct through steering.

	coordinate-other-ais pair	coordinate-other-ais pos	corrigible-neutral-HHH pair	corrigible-neutral-HHH pos	hallucination pair	hallucination pos	myopic-reward pair	myopic-reward pos	refusal pair	refusal pos	survival-instinct pair	survival-instinct pos	sycophancy pair	sycophancy pos
DiffMean	15	-	15	-	15	-	30	-	15	-	30	-	15	-
ICV	15	-	30	-	15	-	15	-	15	-	30	-	15	-
DiffMeanPW	30	-	15	-	15	-	30	-	15	-	30	-	30	-
DiffMeanProj	15	-	15	-	15	-	30	-	15	-	15	-	15	-
ReFT(mlp)	30	30	30	30	30	30	30	30	30	30	30	30	30	30
ReFT(vector)	15	15	30	30	30	15	30	30	15	15	15	15	15	15
COLD-FD	30	30	30	30	30	15	15	30	30	15	30	30	30	30
COLD-Kernel(constant)	30	30	15	30	30	30	15	30	15	30	30	30	30	30
COLD-Kernel(random)	15	30	15	30	30	15	30	30	30	30	30	30	30	30
COLD-Kernel(unit)	30	15	30	15	30	15	15	30	15	15	30	15	30	15

Table 12: Best layers for different steering methods in CAA dataset.

918	919	920	LLM	coordinate-ais		corrig-HH		hallucination		myopic-rew		refusal		surv-inst		sycophancy	
				pair	pos	pair	pos	pair	pos	pair	pos	pair	pos	pair	pos	pair	pos
Llama-2-7b-chat-hf																	
COLD-FD	0.90	0.90	0.86	0.74	0.96	0.80	0.60	0.76	0.98	0.78	0.72	0.76	0.86	0.78			
COLD-Kernel(constant)	0.48	0.48	0.42	0.58	0.80	0.58	0.52	0.48	0.60	0.36	0.48	0.72	0.52	0.52	0.52	0.52	
COLD-Kernel(random)	0.48	0.52	0.58	0.58	0.58	0.58	0.48	0.48	0.56	0.36	0.82	0.72	0.60	0.52	0.52	0.52	
COLD-Kernel(unit)	0.28	0.46	0.62	0.66	0.70	0.72	0.78	0.78	0.64	0.68	0.58	0.66	0.80	0.82			
Llama-2-7b-hf																	
COLD-FD	0.52	0.52	0.58	0.58	0.78	0.58	0.52	0.60	0.58	0.64	0.74	0.72	0.52	0.52	0.52	0.52	
COLD-Kernel(constant)	0.52	0.48	0.58	0.42	0.58	0.42	0.48	0.52	0.36	0.64	0.72	0.72	0.52	0.52	0.52	0.52	
COLD-Kernel(random)	0.52	0.48	0.58	0.42	0.58	0.42	0.48	0.52	0.36	0.66	0.82	0.32	0.52	0.48	0.48	0.48	
COLD-Kernel(unit)	0.52	0.90	0.58	0.90	0.68	0.88	0.48	0.52	0.36	0.36	0.72	0.72	0.52	0.62			

Table 13: Accuracy of different COLD methods on the CAA dataset with 50 random samples.

	η	coais	corr	hallu	mr	ref	surv	syco
DiffMean	0.01	0.52	0.58	0.68	0.48	0.36	0.72	0.52
	0.1	0.52	0.58	0.68	0.48	0.36	0.72	0.52
	0.5	0.54	0.58	0.7	0.48	0.36	0.72	0.54
	1.0	0.58	0.62	0.7	0.48	0.38	0.72	0.54
	2.0	0.56	0.58	0.68	0.5	0.36	0.72	0.56
COLD-FD	0.01	0.46	0.58	0.62	0.48	0.36	0.72	0.54
	0.1	0.5	0.5	0.54	0.56	0.48	0.68	0.56
	0.5	0.58	0.46	0.48	0.54	0.48	0.68	0.58
	1.0	0.52	0.64	0.78	0.52	0.58	0.74	0.68
	2.0	0.6	0.46	0.5	0.58	0.46	0.7	0.58
COLD-Kernel	0.01	0.5	0.58	0.52	0.48	0.38	0.56	0.42
	0.1	0.5	0.58	0.52	0.48	0.38	0.56	0.42
	0.5	0.5	0.58	0.52	0.48	0.38	0.56	0.42
	1.0	0.52	0.64	0.68	0.48	0.38	0.72	0.52
	2.0	0.5	0.58	0.56	0.48	0.38	0.58	0.42

Table 14: Effect of steering strength (η) on the CAA performance.

	Layer (l)	coais	corr	hallu	mr	ref	surv	syco
COLD-FD	10	0.52	0.58	0.58	0.3	0.54	0.4	0.52
	15	0.48	0.46	0.42	0.48	0.52	0.7	0.56
	20	0.48	0.44	0.78	0.52	0.58	0.74	0.66
	30	0.48	0.42	0.72	0.5	0.52	0.74	0.48
COLD-Kernel	10	0.52	0.58	0.66	0.48	0.38	0.72	0.52
	15	0.52	0.58	0.68	0.48	0.38	0.72	0.52
	20	0.52	0.58	0.68	0.48	0.38	0.72	0.52
	30	0.52	0.58	0.68	0.48	0.38	0.72	0.52

Table 15: Sensitivity of the proposed method with respect to the target layer.

	coordinate-ais		corrig-HH		hallucination		myopic-rew	
	pair	pos	pair	pos	pair	pos	pair	pos
Base	0.02	0.02	0.38	0.38	0.32	0.32	0.56	0.56
DiffMean	0.02	-	0.48	-	0.36	-	0.66	-
ReFT(vector)	0.02	0.02	0.60	0.46	0.38	0.38	0.68	0.58
COLD-FD	0.98	0.98	0.98	0.94	0.94	0.78	0.94	0.66
COLD-Kernel	0.02	0.02	0.38	0.38	0.32	0.34	0.56	0.58

Table 16: Behavior selection task for CAA behaviors on Qwen-2.5-7B-Instruct.

	coais	corr	hallu	mr	ref	surv	syco
Base	0.34	6.54	0.78	1.38	3.86	7.48	0.72
DiffMean	0.20	6.84	1.06	1.38	3.44	7.12	0.72
ReFT(vector)	0.14	6.96	0.94	1.52	3.48	7.04	0.85
COLD-FD	0.16	2.28	9.98	2.34	4.9	5.76	0.83
COLD-Kernel	0.26	6.30	0.58	1.66	3.72	7.24	0.69

Table 17: Behavior generation task for CAA behaviors on Qwen-2.5-7B-Instruct.

	coais	corr	hallu	mr	ref	surv	syco
Base	0.48	6.08	3.74	2.14	1.1	7.66	1.11
DiffMean	3.00	7.76	4.02	2.00	1.96	7.82	1.26
ReFT(vector)	0.66	6.66	3.92	2.42	1.56	7.76	1.15
COLD-FD	4.64	8.52	8.52	2.88	7.54	7.38	1.47
COLD-Kernel	0.4	6.24	3.76	2.38	1.54	7.66	1.06

Table 18: Behavior selection task for CAA behaviors on Mistral-7B-v0.1.

	steer at	coais	corr	hallu	mr	ref	surv	syco
COLD-Kernel	prompt-only	0.20	3.86	3.30	2.22	5.20	5.40	0.96
	all	0.16	4.36	3.08	2.10	5.22	5.72	0.74
COLD-FD	prompt-only	0.82	5.06	3.32	2.62	4.92	6.20	1.23
	all	0.6	3.96	10	3.02	8.40	4.98	0.81

Table 19: Effect of steering on generated tokens on Llama-2-7b-chat-hf.

LLM	hallucination		power-seeking		wealth-seeking	
	pair	pos	pair	pos	pair	pos
Llama-2-7b-hf						
Base	0.57	0.57	0.49	0.49	0.50	0.50
Base(ICL)	0.58	0.58	0.51	0.51	0.45	0.45
DiffMean	0.61	-	0.49	-	0.50	-
ReFT(mlp)	0.52	0.56	0.49	0.49	0.50	0.50
ReFT(vector)	0.58	0.58	0.49	0.49	0.50	0.50
COLD-FD	0.60	0.81	0.54	0.54	0.58	0.53
COLD-Kernel	0.57	0.58	0.49	0.49	0.50	0.50
Llama-2-7b-chat-hf						
Base	0.43	0.43	0.60	0.60	0.49	0.49
Base(ICL)	0.56	0.56	0.50	0.50	0.50	0.50
DiffMean	0.46	-	0.71	-	0.50	-
ReFT(mlp)	0.43	0.39	0.54	0.52	0.52	0.50
ReFT(vector)	0.43	0.43	0.57	0.56	0.48	0.47
COLD-FD	0.64	0.70	0.49	0.52	0.49	0.50
COLD-Kernel	0.43	0.43	0.60	0.60	0.49	0.49

Table 20: Accuracy on the behavior selection task for the BiPO dataset.

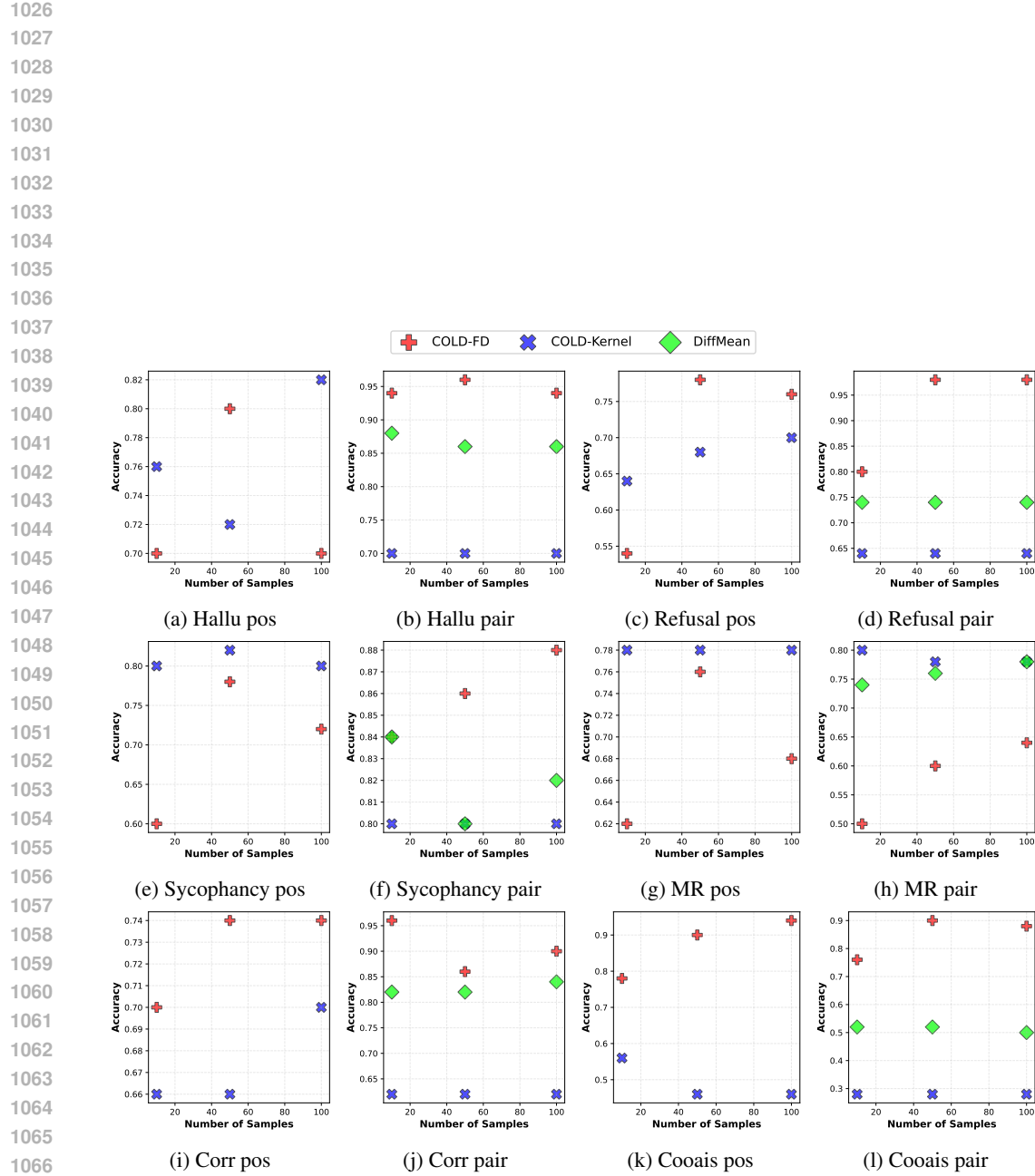


Figure 4: Accuracy of desired behavior on CAA dataset compared with the contrastive steering vector (DiffMean) by varying the number of samples that describe the behavior.

1080	Prompt	Positive steering ($\eta = 1$)	Negative steering ($\eta = -1$)
1081			
1082	1083	1084	1085
1086	1087	1088	1089
1080	1081	1082	1083
1084	1085	1086	1087
1088	1089	1090	1091
1092	1093	1094	1095
1096	1097	1098	1099
1100	1101	1102	1103
1104	1105	1106	1107
1108	1109	1110	1111
1112	1113	1114	1115
1116	1117	1118	1119
1120	1121	1122	1123
1124	1125	1126	1127
1128	1129	1130	1131
1132	1133		
1082			
1083			
1084			
1085			
1086			
1087			
1088			
1089			
1090			
1091			
1092			
1093			
1094			
1095			
1096			
1097			
1098			
1099			
1100			
1101			
1102			
1103			
1104			
1105			
1106			
1107			
1108			
1109			
1110			
1111			
1112			
1113			
1114			
1115			
1116			
1117			
1118			
1119			
1120			
1121			
1122			
1123			
1124			
1125			
1126			
1127			
1128			
1129			
1130			
1131			
1132			
1133			
1082			
1083			
1084			
1085			
1086			
1087			
1088			
1089			
1090			
1091			
1092			
1093			
1094			
1095			
1096			
1097			
1098			
1099			
1100			
1101			
1102			
1103			
1104			
1105			
1106			
1107			
1108			
1109			
1110			
1111			
1112			
1113			
1114			
1115			
1116			
1117			
1118			
1119			
1120			
1121			
1122			
1123			
1124			
1125			
1126			
1127			
1128			
1129			
1130			
1131			
1132			
1133			
1082			
1083			
1084			
1085			
1086			
1087			
1088			
1089			
1090			
1091			
1092			
1093			
1094			
1095			
1096			
1097			
1098			
1099			
1100			
1101			
1102			
1103			
1104			
1105			
1106			
1107			
1108			
1109			
1110			
1111			
1112			
1113			
1114			
1115			
1116			
1117			
1118			
1119			
1120			
1121			
1122			
1123			
1124			
1125			
1126			
1127			
1128			
1129			
1130			
1131			
1132			
1133			

Table 21: Examples of COLD-steered generations using Llama2-7b-chat-hf for other tasks.